Time-of-flight Secondary Ion Mass Spectrometry Investigation of Epoxy Resin Curing Behavior in Real Time

Firas Awaja,[1] Grant van Riessen,[3] Bronwyn Fox,[2] Georgina Kelly,[2] Paul J. Pigram[3]

[1]*School of Physics, University of Sydney, NSW 2006, Sydney, Australia*
[2]*Centre for Material and Fibre Innovation, Geelong Technology Precinct, Deakin University, Geelong, Victoria 3217, Australia*
[3]*Centre for Materials and Surface Science and Department of Physics, La Trobe University, Victoria 3086, Australia*

Received 13 July 2008; accepted 9 November 2008
DOI 10.1002/app.30136
Published online 29 April 2009 in Wiley InterScience (www.interscience.wiley.com).

ABSTRACT: Time-of-flight secondary ion mass spectrometry and principal components analysis were used in real time to monitor the progress of curing reactions on the surface of a diglycidyl ether of bisphenol A (DGEBA) and diglycidyl ether of bisphenol F (DGEBF) epoxy resin blend reacted with the diamine hardener isophorone diamine at different time intervals. Molecular ions in the mass spectra that characterized the curing reactions steps, including blocking, coupling, branching, and crosslinking, were identified. The aliphatic hydrocarbon ions were correlated to the curing reaction rate, and this indicated that coupling and branching occurred much faster than the blocking and crosslinking curing reactions steps. The total conversion of the coupling and branching reaction steps were followed on the basis of changes with time in the relative ion intensity of molecular ions assigned to the DGEBA/DGEBF, aliphatic hydrocarbon, epoxide, and aromatic ring structures. Indicative measures of crosslinking density were monitored through the observation of changes in the ratio of the relative intensities of the aliphatic hydrocarbon and hydroxyl molecular ions over time. The curing reaction conversion was established by the observation of the changes in the relative ion intensity of the molecular ions that were related to the DGEBA/DGEBF molecules. © 2009 Wiley Periodicals, Inc. J Appl Polym Sci 113: 2765–2776, 2009

Key words: adhesives; mass spectrometry; surfaces

INTRODUCTION

Epoxy resins are mainly used as adhesives, in formulations for coating applications, and in polymer composites used in the automotive and aerospace industries.[1–3] The epoxy resin curing/crosslinking reaction is a complex process that involves multiple reaction paths.[4] These reaction paths are not fully understood on the molecular level.[5] The chemical structures of epoxy resins are often the determining factor for the type of application and the associated performance. The molecular structure and nature of epoxy resins depend on the initial ingredients and the curing reaction conditions during the manufacturing process.[3] A crosslinked epoxy resin is usually obtained via the curing reaction of a bifunctional epoxide such as diglycidyl ether of bisphenol A (DGEBA) or diglycidyl ether of bisphenol F (DGEBF) with a multifunctional crosslinking/curing agent (hardener). Amine-type curing agents are the most widely used crosslinking agents. They are tetrafunctional, with the hydrogen atoms on the sides of the nitrogen atoms being the reacting units. Nitrogen atoms react with the epoxy group on the resin, resulting in a new carbon bond and a hydroxyl-functional group.[3] The tetrafunctionality of the crosslinking agent means that it can react with four epoxide groups, and this eventually results in a crosslinked structure. The final product is ideally a fully crosslinked network, that is, effectively a single, giant molecule. However, linear and branched chains coexist as a result of incomplete reaction conversion and the nature of the curing reaction path, and they affect final product specifications.[3] Revealing the molecular information for these chains will enhance our ability to control and optimize their amount and integration in the final product.

Monitoring the progress of the epoxy resin curing reaction enables more control over the final product specifications. Furthermore, the characterization of the epoxy resin molecular structure will provide insight into the structure–property relationships and resistance against environmental degradation. In this

Correspondence to: F. Awaja (firas@physics.usyd.edu.au).

work, the progress of the curing reaction of a DGEBA and DGEBF epoxy resin blend reacted with an isophorone diamine (IPD) based hardener was followed with time-of-flight secondary ion mass spectrometry (ToF-SIMS). Molecular changes were revealed as a function of time for the curing reaction of the epoxy resin and IPD hardener.

Many offline and online techniques for monitoring the progress of curing reactions have been reported.[3,6–11] Offline methods such as titration, specific gravity, and differential scanning calorimetry (DSC) measurements have been used, with samples taken at certain times during the curing reaction and tested separately.[5,12] Properties associated with reaction kinetics such as the reaction activation energy, frequency factor, and reaction order and kinetics analysis are often determined with DSC.[4,5,12–17] A significant number of researchers have attempted to explain the reaction chemistry and physics of the DGEBA/diamine mixture.[5,14,18] The curing reaction of DGEBA as a function of various imide–amine and diamine hardener concentrations with DSC has been reported previously.[4,13] Pichaude et al.[14] reported the effects of the hydroxyl content on the curing kinetics of DGEBA with IPD as a hardener. López-Quintela et al.[18] studied the cis/trans reactivity of the DGEBA epoxy/diamine blend. The cured resin morphology that determines its properties is dependent on the nature and rate of the crosslinking reaction between the resin and the hardener.[17] Other studies have shown that the curing of the epoxy resin is dependent on the structure of the hardener and its concentration.[13]

Online methods involve the use of small sensors that are inserted into the materials during curing and transmit signals to an external instrument for monitoring the curing reaction progress. A method called low-frequency dielectrometry measures permanent dipoles within the structure and the mobility of impurities in the resin matrix. These quantities correlate with the resin viscosity and mechanical rigidity, which in turn are related to the reaction conversion.[6,7] Infrared spectroscopy and Raman spectroscopy have been used in combination with optical fibers implanted in the curing resin to transmit spectral information to an outside monitoring system.[8–11]

In this study, we used ToF-SIMS to establish real-time monitoring of the DGEBA/DGEBF epoxy resin/IPD curing reaction. ToF-SIMS is a technique that, when used in real-time measurements, has the potential to provide rich information about a wide range of molecular changes as a function of the curing reaction time. ToF-SIMS was used to follow the progress of the curing reaction of a DGEBA/DGEBF-based epoxy resin and an IPD-based hardener, and we took advantage of the fact that ToF-SIMS, unlike the aforementioned monitoring methods, is sensitive to changes in the composition and molecular structure on the surface of materials. Variations in the intensities of peaks characteristic of ion fragments of the resin and hardener and their reaction products are compared with univariate and multivariate techniques. The ToF-SIMS technique has been used previously to investigate the molecular changes of thermosetting resins. For example, Coullerez et al.[19] used ToF-SIMS to investigate a melamine–formaldehyde resin (uncured and fully cured). They showed that by an inspection of the surface with ToF-SIMS, further information was revealed regarding the chemical structure of the melamine–formaldehyde resin. Rattana et al.[20] reported on the kinetics and thermodynamics of adsorption and thermodynamics of DGEBA epoxy resin molecules on aluminum substrates treated with the organosilane *g*-glycidoxypropyltrimethoxysilane. Using ToF-SIMS as an analytical tool, they established the fractional monolayer coverage of DGEBA molecules.

ToF-SIMS data are complex in nature, and the analysis may be significantly simplified by multivariate techniques such as principal components analysis (PCA).[21,22] The data that are collected from ToF-SIMS are normally pretreated before the application of PCA. Data pretreatment, such as scaling, ensures that the variance in the measured values is due to chemical differences between samples and not an artifact of variations in the total secondary ion current or detector efficiency.[21,22]

EXPERIMENTAL

Materials

The epoxy resin Kinetix R246TX (ATL Composites, Southport, Queensland, Australia) was used in this study. The resin mainly consists of DGEBA blended with DGEBF and aliphatic glycidyl ether as a functional diluent. A superfast hardener (Kinetix H126, ATL Composites) manufactured to cure at room temperature with IPD as the main ingredient was employed. Figure 1 shows the chemical names and structures of the main resin and hardener ingredients.

ToF-SIMS

ToF-SIMS analyses were performed with a ToF-SIMS IV instrument (Ion-TOF GmbH, Germany) equipped with a reflectron time-of-flight mass analyzer, a Bi_3^+ ion gun (25 keV), and a pulsed electron flood source for charge compensation. The primary pulsed ion beam current was 1.1 pA, and the primary ion dose density was below the dynamic secondary ion mass spectrometry limit of 10^{13} ions/cm^2. Positive high mass resolution (>7500 at $m/z = 29$) spectra were

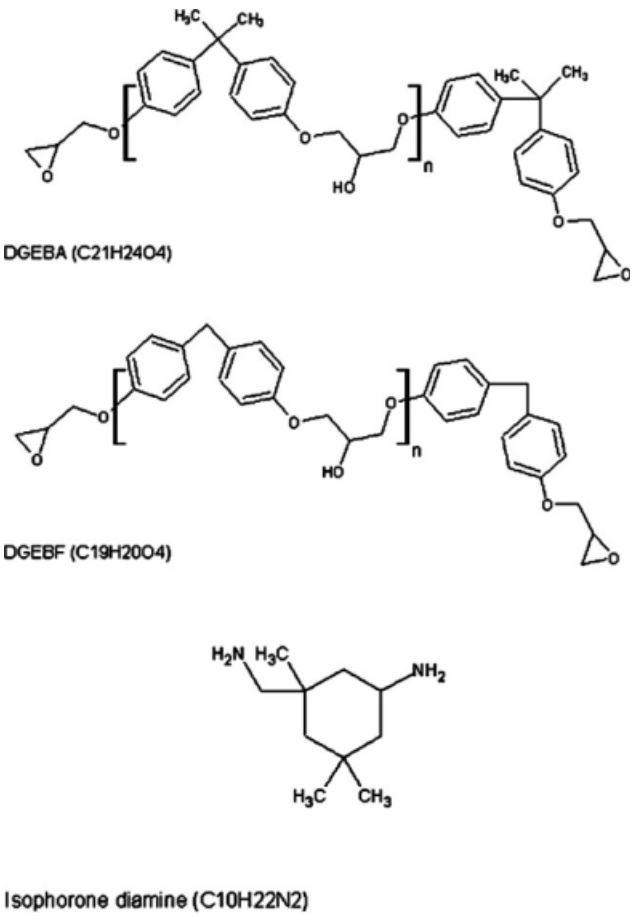

Figure 1 Molecular structures of the noncrosslinked poly-DGEBA, DGEBF resin, and IPD hardener.

acquired for 100 μm × 100 μm areas from fresh spots for each time interval with a cycle time of 100 μs.

The resin and hardener were mixed for 10 min at a ratio of 4 : 1, as recommended by the producer. The mixture was spin-coated onto a silicon wafer and immediately transferred to the ToF-SIMS sample introduction chamber, which was evacuated. When a sufficiently low vacuum was achieved, the sample was transferred to the main vacuum chamber, in which a vacuum pressure better than 2×10^{-8} torr was maintained.

The curing of the epoxy resins was known to proceed rapidly during the first hour after initiation, as indicated by the resin and hardener producer. The experimental schedule was designed both to distribute data points across a 24-h period and to provide additional data points during the period of most rapid chemical change. The time domains were selected on the basis of the main events in the curing process of this resin and hardener system as recommended by the resin producer. The first time domain was on and after the pot lifetime, the second domain was on and after the 4-h thin laminate open time, and 24 h was the final cure time. Positive-ion spectra were acquired 40 min after the resin and hardener were mixed and applied to the silicon wafer. Fifteen spectra were subsequently obtained at 4–6-min intervals for about 30 min, each from a fresh area of the sample. After about 4 h, another five spectra were obtained at similar intervals. One final spectrum was acquired after 24 h while the sample remained in the chamber.

Data analysis

The peaks for data analysis were selected initially on the basis of reference libraries and previous assignments in the literature for DGEBA, DGEBF, and IPD molecules. Furthermore, peaks were assigned with the library and the exact mass calculator tool in Ionspec software (Ion-TOF) to identify contaminant peaks, including the hydrocarbon peaks, and peaks that were likely to correspond to fragments of the resin/hardener that were not listed in the literature. All the significant peaks above the baseline in the m/z range of 0–300 were selected. Significant peak intensities that could be resolved and related to the DGEBA, DGEBF, and IPD molecules in the m/z range of 300–650 were also included. The mass spectra were calibrated with a series of hydrocarbon (C_xH_y) peaks up to $m/z = 105$.

The data were grouped in a matrix, and the columns in the matrix were normalized to the total intensity. The matrix was mean-centered before it was used for PCA. The mean-centered matrix was used for PCA. PCA is a multivariate technique used to ease the interpretation of large amounts of data such as those generated by ToF-SIMS and to identify meaningful variables. It does so by compressing a large number of variables into a smaller number of principal components. The principal components are calculated statistically to group the main variances in the data and sort them in order of magnitude with the singular value decomposition of the data set. PCA was performed with code developed in house and with functions provided in the Stats package (version 2.5.1) for R, a language and environment for statistical computing and graphics, on the basis of the covariance method algorithm described in detail by Martens and Naes.[23] The covariance matrix is calculated from the mean-centered matrix, and the eigenvalues are extracted from the covariance matrix and sorted. The eigenvectors are calculated in the next step with the covariance matrix and the eigenvalues. The eigenvalues are the percentages of information that each eigenvector collects from the original dataset. When they are sorted in order, eigenvectors in order of significance can also be generated. Normally, the first few eigenvectors collect the main information in the data set, whereas the remaining eigenvectors collect the residual

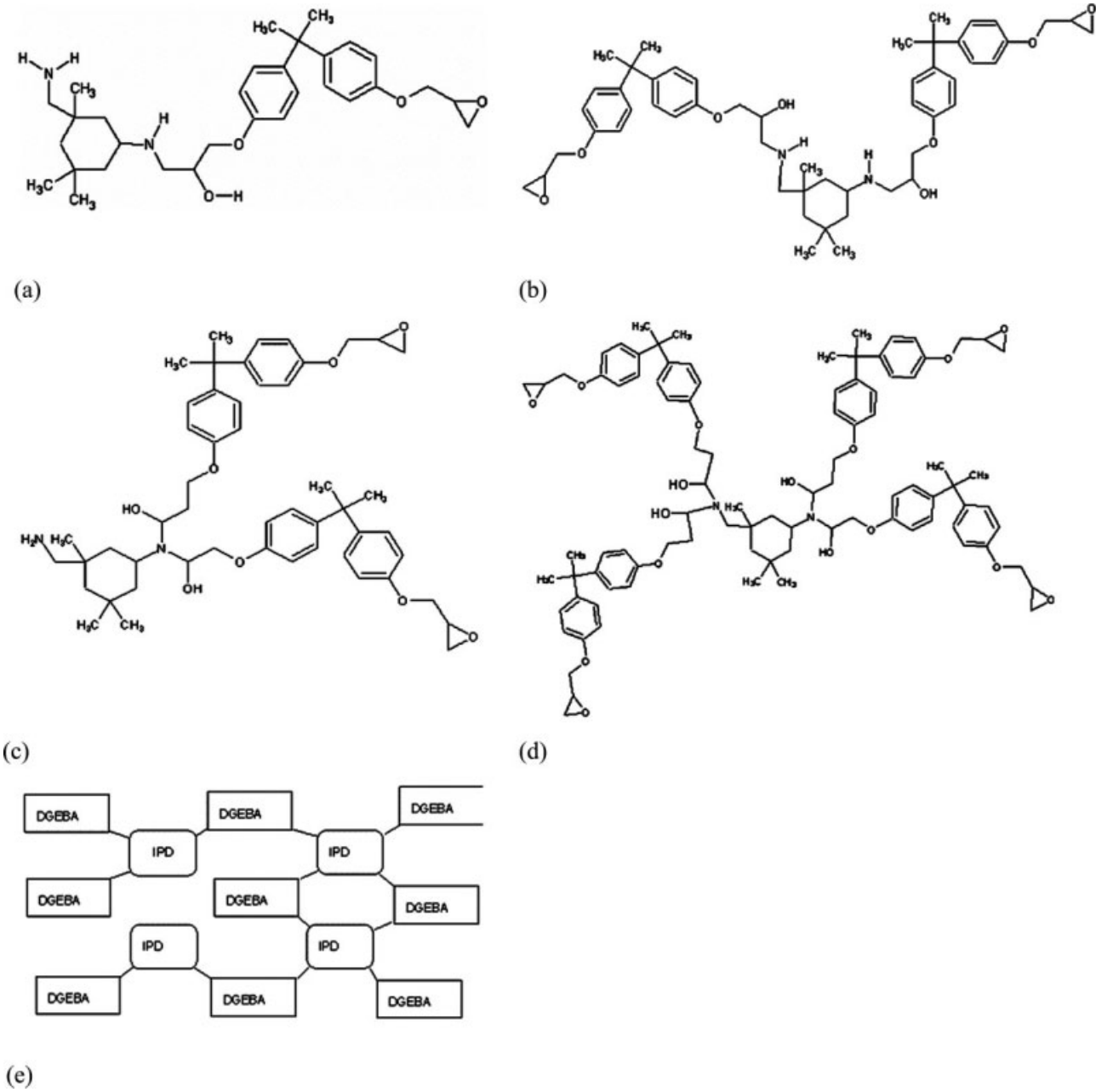

Figure 2 (a–d) Structures produced by the epoxy resin curing reactions (blocking, linear coupling, parallel coupling, and branching, respectively) and (e) representation of a model crosslinking network.

information from the data set. The principal components are then calculated by multiplication of the mean-centered original matrix by the eigenvectors. PCA is normally discussed in terms of scores and loading plots. The score plots are the principal components plotted against each other or against the data set main variables. The loadings are the relative contributions of the mass peaks in the peak list to the principal components. The loading plots are the eigenvectors plotted against the spectral mass values.

RESULTS AND DISCUSSION

Curing stoichiometry information for the DGEBA-based epoxy resin indicates that the reaction pathway starts with the linking of one DGEBA molecule at a time to the IPD hardener molecule through the transformation of the hydrogen atom of the amine functionality.[3] A bifunctional epoxy resin reacting with tetrafunctional crosslinking agents should result in three reaction steps, namely, coupling, branching, and crosslinking.[24–31] Figure 2 shows the

proposed structures produced by each reaction step for the reaction of DGEBA and IPD molecules. Initially, molecular blocking occurs when one DGEBA or DGEBF molecule is linked to one IPD molecule. A coupling reaction step occurs when two DGEBA or DGEBF molecules are linked to one IPD molecule. This coupling reaction step depends on the hardener concentration and molecular mobility of the resin and hardener reactive molecules.[24] The linkage could be linear [i.e., the epoxy resin molecules are linked on each side of the amine group; Fig. 2(b)] or parallel [both molecules are linked to the same amine group; Fig. 2(c)]. The branching reaction step is the development of the coupling reaction step in which more than two DGEBA molecules are connected to one IPD molecule, as shown in Figure 2(d). Crosslinking occurs when all these reactions occur to create networks involving many DGEBA molecules connected to multiple IPD molecules. The ultimate goal of the epoxy resin curing reaction is to have one large network in which the IPD molecules are fully reacted and integrated into the final structure. Naturally, the curing reactions coexist and compete with one another and also are expected to be affected by the chain mobility and local hardener concentration.

The fragmentation and ionization upon primary ion bombardment of the DGEBA epoxy resin and IPD molecules and their changes with crosslinking are complex; however, a simplified argument is developed here to understand the ToF-SIMS spectra. It is hypothesized that primary ion bombardment generates secondary ions in three energy regions.[32] In the first region, violent fragmentation occurs in a narrow volume beneath the direct impact of the primary ion. As a result, aliphatic radical ions (e.g., $C_4H_9^+$, $C_2H_5^+$, and $C_3H_7^+$) are most likely to be the products of the primary ion interaction as a result [Fig. 3(a)]. Around this volume is another zone in which the primary ion energy decreases, yielding neutral analyte fragments and, to a small extent, fragment ions.[32] The double- and single-ring ions [Fig. 3(b)] are believed to be examples of fragments in this region for the DGEBA resin. The third region receives even lower energy primary ions, which lead to the fragmentation of large and highly structured fragments [Fig. 3(c)]. Examples of the fragments in this region are the DGEBA molecular ions ($C_{21}H_{24}O_4^+$) and derivative ions.

On the basis of this fragmentation proposition, as the curing reaction progresses, epoxy resin networks are building and establishing stronger and denser crosslinks with integrated IPD molecules. It is anticipated that the relative abundance of low-molecular-weight aliphatic radical ions from the DGEBA/DGEBF and IPD network will be much higher in comparison with other structures in the fully cured network. The energy that is required to fragment high-molecular-weight structural ions in the second and third regions will be insufficient because of stronger molecular interactions.

Time-of-flight mass spectrometry is a high-resolution technique allowing the analyst to distinguish many discrete molecular fragment ions with the same notional integer mass. These properties make ToF-SIMS a remarkably powerful tool for examining

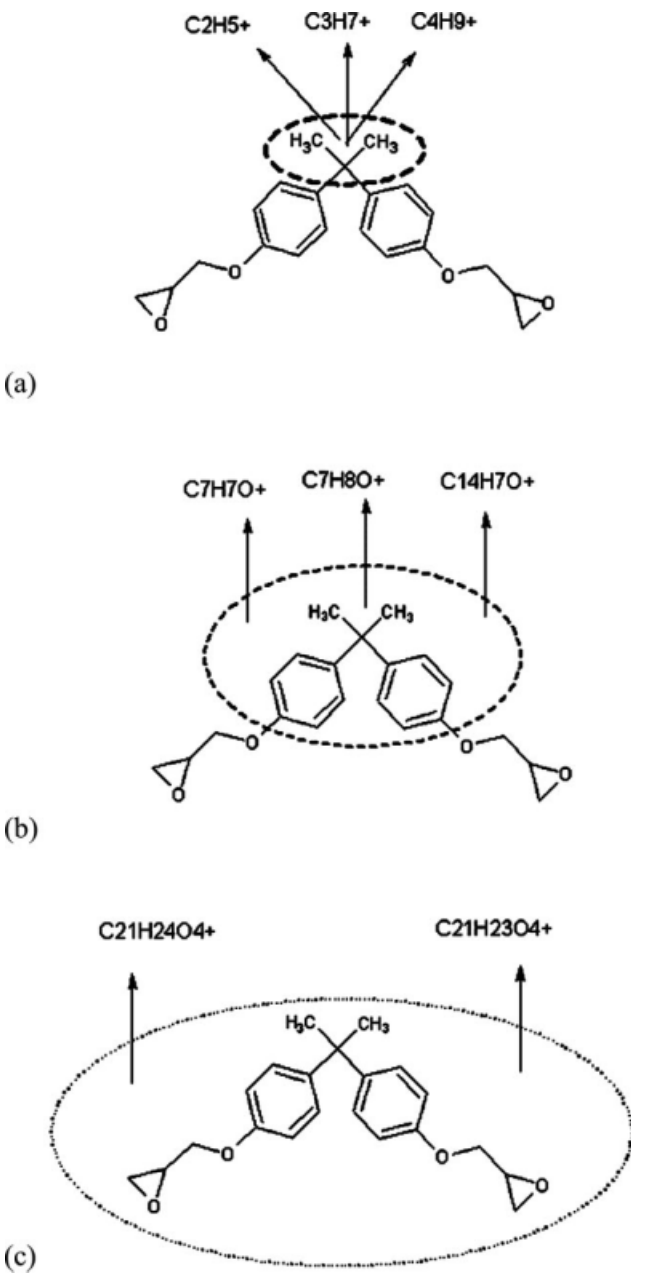

Figure 3 Model fragmentation of the primary ion and examples of the resulting secondary ions on the DGEBA molecule for the (a) violent fragmentation region, (b) low-energy fragmentation region, and (c) structural fragmentation region.

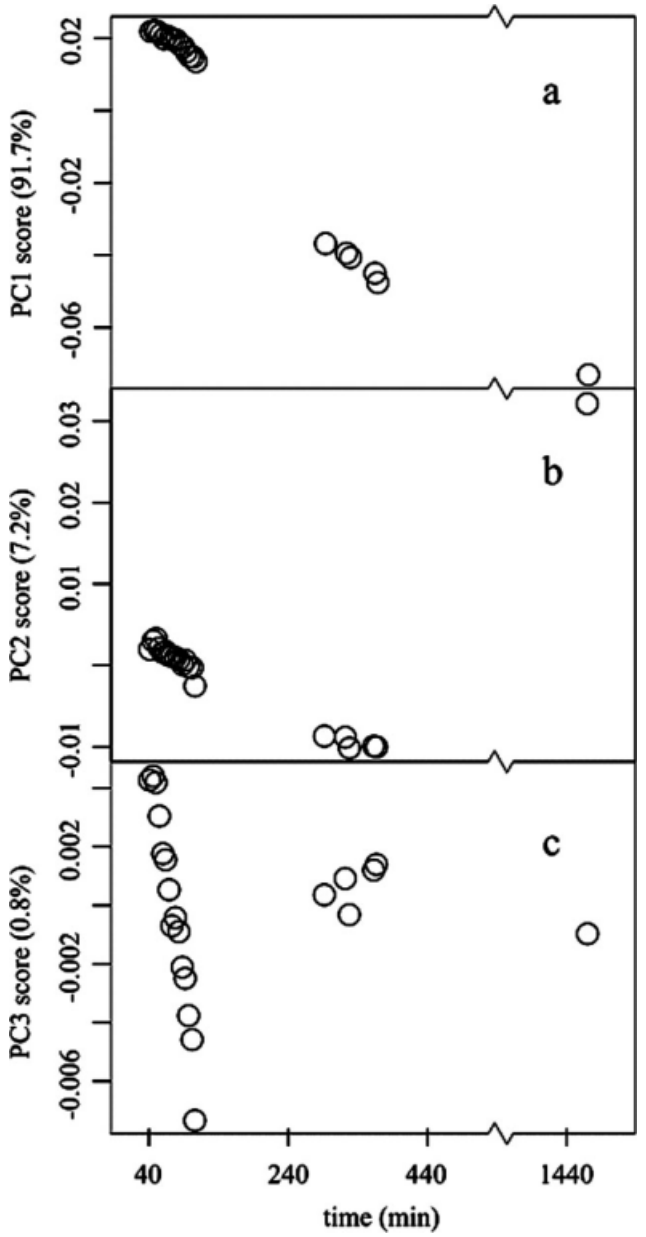

Figure 4 PCA score plots for (a) PC1 (91.72%), (b) PC2 (7.2%), and (c) PC3 (0.8%) with ToF-SIMS spectra for all time domains. The percentage of total variance collected in each principal component is indicated in parentheses.

and understanding polymer systems. However, the complexity of the data requires novel approaches for extracting information about the structure and function of the analyzed sample. The aim of PCA of ToF-SIMS data is to reduce the number of variables (relative peak intensities), or degrees of freedom, to fewer components that represent the major chemical phenomena, such as changes in the composition or structure, associated with the sample set and its treatment. PCA is ideally suited for revealing variance in sample sets, both between treatments and within groups of replicate samples, and for identifying the mass spectral peaks contributing to this variance.

PCA was conducted initially with a data set constructed by the inclusion of the normalized ToF-SIMS peak intensities obtained at all time intervals, that is, from 40 to 1529 min. Figure 4 shows the score plots of the first principal component (PC1), which captured 91.7% of the total variance between observations, the second principal component (PC2), which captured another 7.2% of the variance, and the third principal component (PC3), which captured 0.8% of the data information. The remaining principal components gathered trivial information about the data set and hence were ignored. Figure 5 shows the PCA loading plots for PC1, PC2, and PC3. PCA enabled discrimination between the three time domains based on the ToF-SIMS spectral information. The first domain consists only of observations during the time frame between 40 and 105 min. The second domain contains observations from the second time frame between 291 and 366 min. The final domain contains a single observation made after 24 h.

PC1 clearly distinguishes three domains and captures information related to major phenomena with a variance trend that decreases as the curing reaction time increases. Figure 5(a) shows the PC1 loadings in relation to the mass of the selected peaks. The peaks whose variations contribute most significantly to PC1 are marked in the loading plot. The highest variance captured by PC1 is for the aliphatic hydrocarbon ions of $C_4H_9^+$, $C_2H_5^+$ $C_3H_7^+$, $C_3H_5^+$, and $C_4H_7^+$. Univariate plots of $C_4H_9^+$, $C_2H_5^+$, and $C_3H_7^+$ ions show an increase in the intensity as a function of the curing reaction time, as shown in

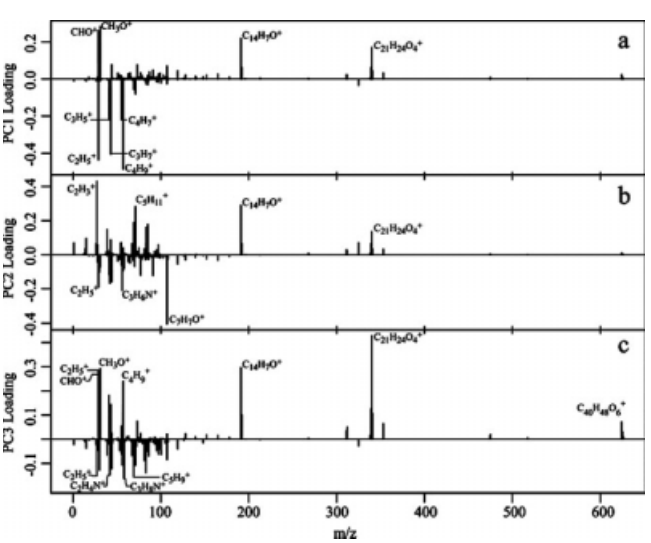

Figure 5 PCA loading plots of (a) PC1, (b) PC2, and (c) PC3 with ToF-SIMS spectra for all time domains.

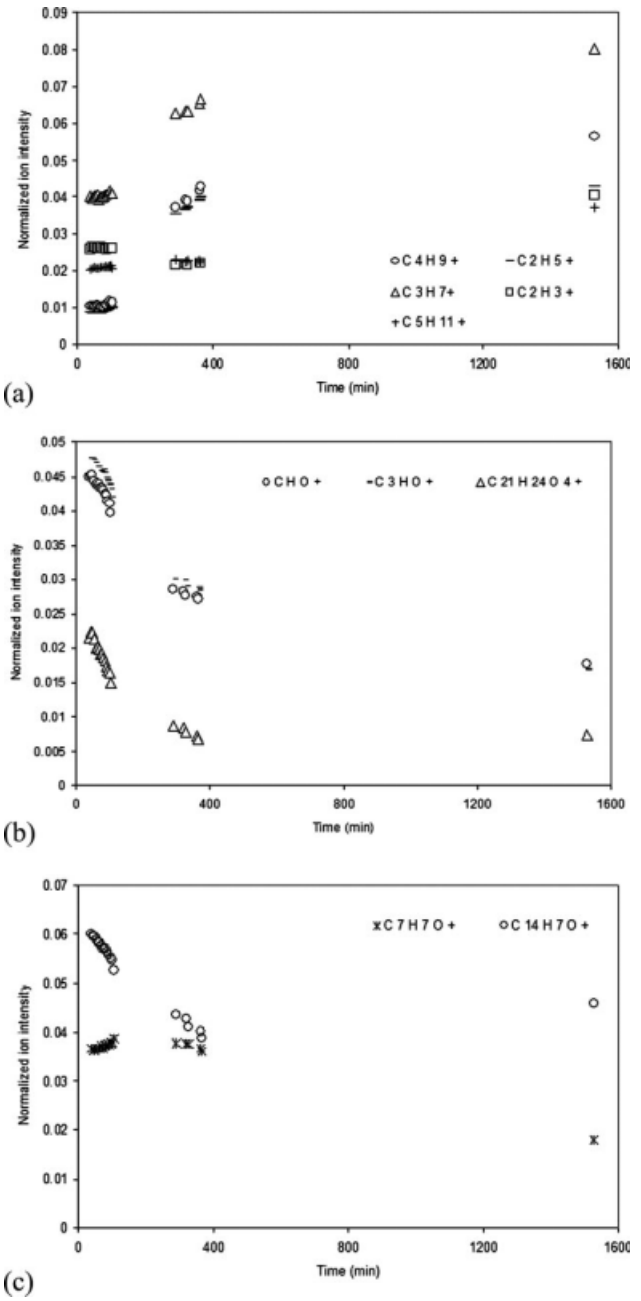

Figure 6 Variation in the intensity of secondary ion peaks of samples that showed significant variance by PCA.

Figure 6(a). The aliphatic hydrocarbon peak intensities increase rapidly between the first and second domains of the samples, whereas they show a lower increase in the rate moving toward the last sample. The second domain of samples shows a higher rate of increase than the first domain. In line with the primary ion fragmentation hypothesis for the DEGBA molecule explained previously, the aliphatic hydrocarbon relative secondary ion yields are proportional to the curing reaction time. As the branching and crosslinking reactions develop and produce denser structures, relative secondary ion yields for the aliphatic radical ions increase as other larger molecular structures result in less fragmentation. The increase of the hydrocarbon ions is indicative of the completeness of the curing reaction. Previous studies[33] have shown that fully cured epoxy resins exhibit higher aliphatic hydrocarbon ion intensity than the resins and hardener molecules themselves.

The hydroxyl groups CHO^+ and CH_3O^+ also show large loadings, which indicate that they contributed significantly to the variance in the data in the PC1 score plot. The hydroxyl-functional groups are of particular interest as their change in concentration indicates the progression of the coupling reaction step of the curing reaction. These ions are fragments of the epoxide group of the DGEBA/DGEBF molecules, and their concentration is believed to be proportional to the concentration of the epoxide group in the curing resin. The epoxide groups are consumed via the linkage of the DGEBA/DGEBF molecules, in which they are the terminal groups, with the IPD molecules. A higher curing reaction conversion results in lower epoxide ion intensities. The intensity of these ions decreases as a function of the reaction time, as shown in Figure 6(b). The decrease in the relative peak intensities of these ions indicates the consumption of the epoxide group by the coupling and branching curing reaction steps. Figure 6(b) shows that the relative peak intensity of these ions decreases rapidly as time progresses, and the rate of reduction decreases toward the last sample. Hence, the coupling and branching of DEGBA/DGEBF and IPD molecules start at a high rate and subside as the terminal functional groups decrease in number. The first domain of samples shows a steeper decrease in the number of hydroxyl ions than the second domain of the samples. Figure 5(a) shows that the aliphatic hydrocarbon ions point in the direction opposite of that of the hydroxyl ions in the loading plot. Figure 6(a,b) shows that the aliphatic hydrocarbon relative ion intensities have a trend almost the opposite of that of the hydroxyl relative ion intensities. The coupling and branching reaction rates and their correlation to the overall curing reaction hence can be characterized, depending on the increase or decrease in the rate of the aliphatic hydrocarbon and hydroxyl ions, as described previously. The time in which coupling and branching reaction steps are initiated and completed can be followed on the basis of the observation of the aliphatic hydrocarbon and epoxide group ion intensity changes as a function of time. According to the primary ion fragmentation hypothesis, the ratio of the relative ion intensity of the aliphatic hydrocarbon and hydroxyl ions indicates the resin crosslinking density. Structures with higher crosslinking density produce more aliphatic ions and fewer hydroxyl ions than low-density crosslinks.

The variance of intensity of the molecular ion, which is related to the DGEBA molecule ($C_{21}H_{24}O_4^+$), has a significant influence on the separation of samples by PC1, as shown in Figure 5(a). The $C_{21}H_{24}O_4^+$ ion variance points in the same direction as the hydroxyl and double-ring ions in the loading plot [Fig. 5(a)], and this indicates that changes in the intensity of the peaks related to DGEBA and to $C_{21}H_{24}O_4^+$ occur together. The DGEBA molecule relative ion peak intensity decreases rapidly in the early stages in the first domain of samples, and then the intensity decreases at a lower rate in the second domain of samples. It remains unchanged for the last sample, as shown in Figure 6(b,c). The rapid consumption of the DGEBA molecule is an indication of the coupling and branching reaction steps, as shown in the first domain of spectra up to 105 min. The rate of consumption slows significantly in the second set. The last sample at 1529 min shows no increase in consumption of the DGEBA molecule. This trend explains the transformation of the coupling reaction step into branching and crosslinking reaction steps. Furthermore, the DGEBA ion intensity diminishes to insignificant counts in the fully cured resin,[33] so the DGEBA relative ion intensity may be used as a measure of the curing reaction conversion and the completeness of the coupling and branching reaction steps.

PC2 captures the variance indicating phenomena (reactions) that decrease between the first and second time domains at almost the same rate but increase sharply toward the 24-h sample. Figure 5(b) shows that the relative ion intensities of $C_7H_7O^+$ and $C_{14}H_7O^+$, which are assigned to the single- and double-ring formation in the DGEBA/DGEBF molecules, contribute significantly to the variance captured by PC2. The aromatic ring fragments of $C_7H_7O^+$ (appearing in PC2) and $C_{14}H_7O^+$ (appearing in both PC1 and PC2) of the main DGEBA structure are related to the progression of the reaction by limited fragmentation as the crosslinking moves to a higher order. These ions fragment more easily when the curing reaction is in the coupling and branching stage and fragment with more difficulty as the networks start to formulate. The ion that is assigned to the double-ring molecule ($C_{14}H_7O^+$) will obviously require higher energy to fragment than the single-ring ion ($C_7H_7O^+$) because of the lower molecular weight. Figure 5(c) shows that these ions have variance in opposite directions. Furthermore, Figure 6(c) shows that the $C_7H_7O^+$ ion peak intensity increases initially in the first time domain and decreases slightly and steadily toward the second and third domains of the samples. The $C_{14}H_7O^+$ relative ion peak intensity decreases sharply with time for the first and second domains and then increases slightly toward the last sample. Furthermore, the double-ring ion ($C_{14}H_7O^+$) is not detected when the resin is fully cured.[33] Hence, the relative ion intensity of the single- and double-ring ions may be used as a measure of the unreacted DGEBA molecule fraction. Other significant contributions include the $C_2H_3^+$ and $C_5H_{11}^+$ aliphatic hydrocarbon ions. The aliphatic hydrocarbon ion peaks contribute significantly to the separation of time domains in PC2. The fact that these peaks contribute only to PC2 and not to PC1 and the high separation of the last sample in PC2 indicate that these ions are forming at a later stage of the curing reaction. PC2 loadings also feature new aliphatic hydrocarbon ions of $C_2H_3^+$ and $C_5H_{11}^+$, which appear in the direction opposite of that of the residual variance of the main aliphatic hydrocarbon ions featured mainly in PC1, such as $C_2H_5^+$ and $C_4H_9^+$. Figure 6(a) shows that $C_2H_3^+$ has a different trend in the first and second time domains of the samples than the rest of the aliphatic hydrocarbon ions as it decreases in intensity as the curing reaction time increases. Then, the relative ion intensity of $C_2H_3^+$ increases as time progresses. This indicates that these molecules fragment in the later stages of the crosslinking reaction.

Information collected in PC3 separate the 25-h sample from the rest of the samples. The information captured in PC3 shows that the first domain of spectra extends in a trend different from that of the second domain, in which the spectra are gathered closely. This indicates that PC3 captures a variance related to a physical phenomenon that is more important in the first domain of samples. However, the domain overlap indicates that the phenomena occur in all samples at all times, though at different rates. This phenomenon is revealed in the PC3 loading graph [Fig. 5(c)], which shows a high variance in the relative ion intensity of the DGEBA ($C_{21}H_{24}O_4^+$) molecule because the consumption of the DGEBA molecule is related to the coupling and branching reaction steps. PC3 reveals that coupling and branching reactions dominate the crosslinking reaction in all the spectra up to 105 min. These curing reaction steps slow gradually in favor of the crosslinking reaction step. The latter eventually dominates, as we see in the change in the trend in the second domain of spectra.

Additional PCA was conducted with data sets constructed from the separated time domains described previously. Because the different time domains correspond to different curing reaction stages, it is useful to explain PCA at each stage. Initially, a data matrix that contained the normalized ToF-SIMS spectra taken at times ranging from 40 to 105 min was used. Figure 7 shows the PCA score plots for the first three principal components. PC1 captured 89.5% of the variance information, and PC2

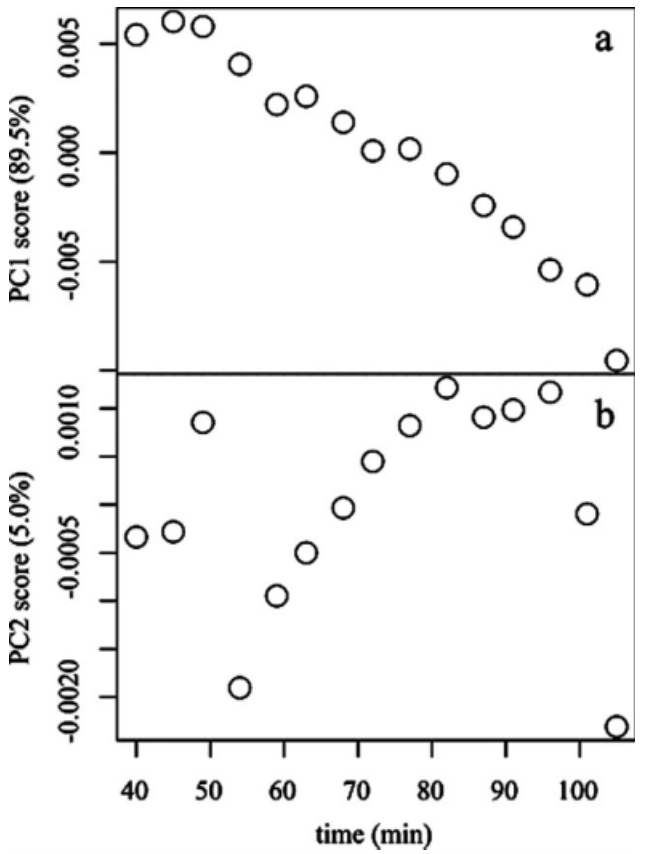

Figure 7 PCA score plots of (a) PC1 (89.5%) and (b) PC2 (5.0%) with ToF-SIMS spectra for first time domain samples only. The percentage of total variance collected in each principal component is indicated in parentheses.

captured another 5.0%. The remaining principal components were insignificant. Figure 8 shows the PCA loading plots for the two principal components with the peak assignments of the most significant peak intensities that contributed to PC1 and PC2. Figure 9 shows the univariate representation of the most significant ion peak intensities in PC1 and PC2 as evaluated by PCA.

PC1 shows a trend of a steady decrease as a function of time. PC2 shows a trend in the middle time section of samples while having outlying readings in the early and later time sections, as shown in Figure 7(b). The ion peak intensities related to the DGEBA molecule ($C_{21}H_{24}O_4^+$) and the double-ring structure ($C_{14}H_7O^+$) contribute the most to the PC1 loadings, as shown in Figure 8(a). The molecular ions arising from the epoxide group (CHO^+ and CH_3O^+) come third in line as the most significant variance in the PC1 loadings. All these ions are featured in the same positive direction in the loading plot. Finally, there is some contribution from aliphatic hydrocarbon ions of $C_4H_7^+$ and $C_3H_8^+$, carbon–nitrogen ions of $C_2H_4N^+$ and $C_3H_8N^+$, and the single-ring ion of $C_7H_7O^+$, which are all featured in the negative

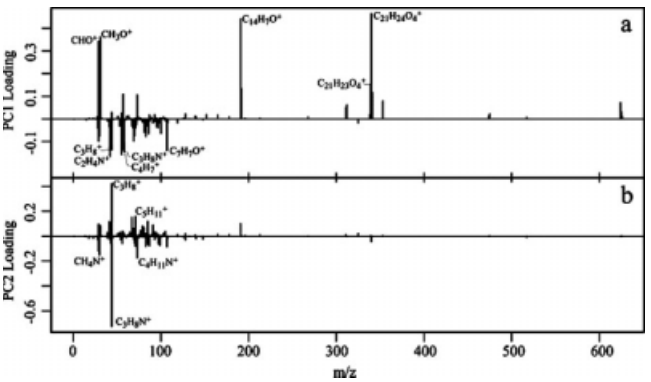

Figure 8 PCA loading plots of (a) PC1 and (b) PC2 with ToF-SIMS spectra for first time domain samples.

direction of the loading plot. An ion fragment of the DEGBA molecule ($C_{21}H_{23}O_4^+$) is also captured as a peak with noticeable variance over the samples. A comparison of Figures 7(a) and 8(a) shows that the strongly contributing ions, such as $C_{21}H_{24}O_4^+$, $C_{14}H_7O^+$, and CHO^+ and CH_3O^+, must be responsible for the decreasing trend shown in the score plot [Fig. 7(a)]. This confirms the earlier conclusion that the coupling and branching reaction steps start first, and their rate can be followed by the observation of the strongly contributing ions, as noted previously, in this time frame. The crosslinking reaction has not developed significantly, as indicated by the lower aliphatic hydrocarbon variance.

Figure 9 shows a univariate plot of the most significant peak intensities contributing to the PCA loadings. The ion peak intensity of the molecular ion of $C_{21}H_{24}O_4^+$ shows a steady decrease with time, which is consistent with uniform and slow coupling/branching reactions within this time margin. The aromatic ring fragments of $C_7H_7O^+$ and

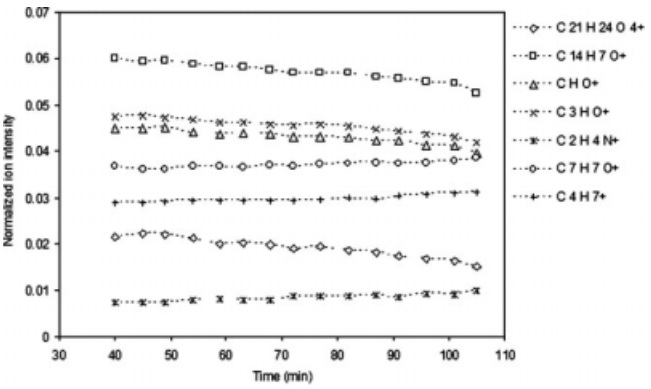

Figure 9 Variation in the intensity of secondary ion peaks of first time domain samples that showed significant variance by PCA.

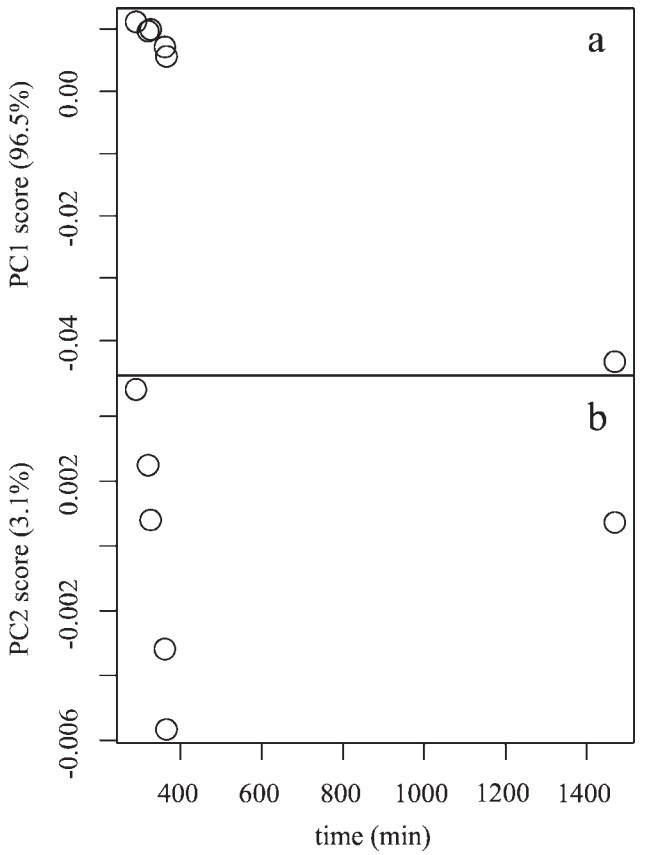

Figure 10 PCA score plots of (a) PC1 (96.50%) and (b) PC2 (3.1%) with ToF-SIMS spectra for the second and third domains.

$C_{14}H_7O^+$ (contributing to PC1 only) also indicate the progression of the reaction, as explained previously. However, the $C_{14}H_7O^+$ aromatic ion is more significant than the $C_7H_7O^+$ ion because of the relative ease of fragmenting more structured ions when no complex networks have yet been established. The ion fragmentation of the epoxy-functional groups (CHO^+ and CH_3O^+) shows a similar trend of a steady decline to $C_{21}H_{24}O_4^+$, a representation of the progress of the coupling and branching reaction steps. The amine groups $C_2H_4N^+$ and $C_3H_8N^+$ (appearing in PC1) and $C_2H_6N^+$ (appearing in PC2) show less significance variance and are products of the coupling reaction step (Fig. 9). These ions increase in intensity as the curing reaction progresses. The hydrocarbon ion $C_4H_7^+$ shows a slight increase in intensity as the time progresses.

The physical phenomena that occur within the first domain of samples include the establishment of the coupling reactions, as indicated by the steady decrease of the DEGBA ion. The increase of $C_2H_4N^+$, as shown in Figure 9, indicates the establishment of the blocking reaction between the IPD molecule and the DGEBA and DGEBF molecules within the structure.

Further PCA was conducted for the second domain of samples with data-containing spectra collected at times ranging from 291 to 1529 min. Figure 10 shows the PCA score plots for data in this time period. PC1 captured 96.5% of the variance, and PC2 captured 3.1%. The higher order principal components were insignificant. The score plots show that PC1 represents a major phenomena in which the samples follow a trend that decreases sharply as the time increases toward the sample at 1529 min. PC2 shows that the samples in the second domain spread all over the range, and it overlaps the last domain sample.

Figure 11 shows the PCA loading plots of PC1 and PC2 for data in the aforementioned time period,

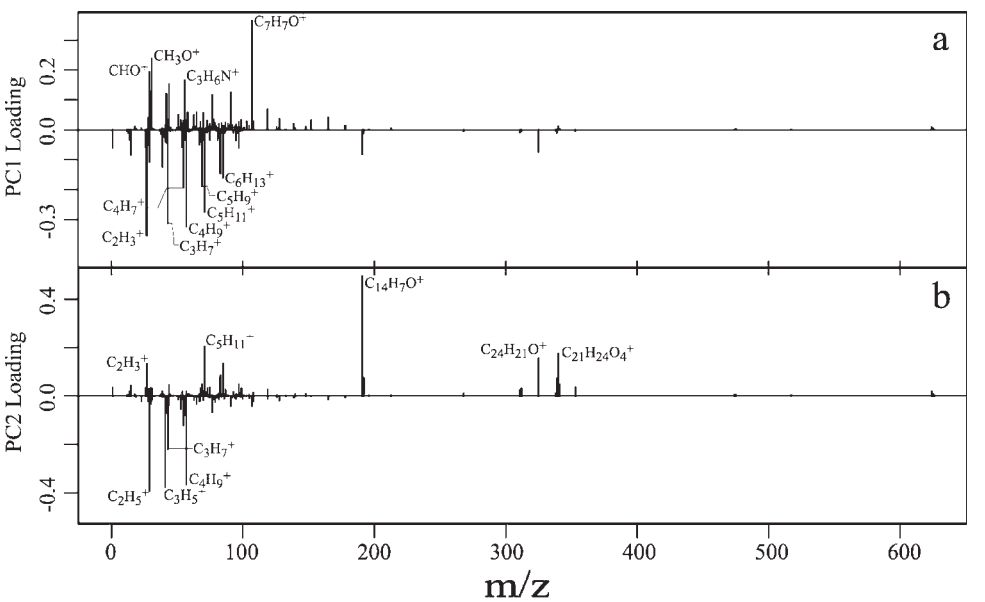

Figure 11 PCA loading plots of (a) PC1 and (b) PC2 with ToF-SIMS spectra for second and third time domain samples.

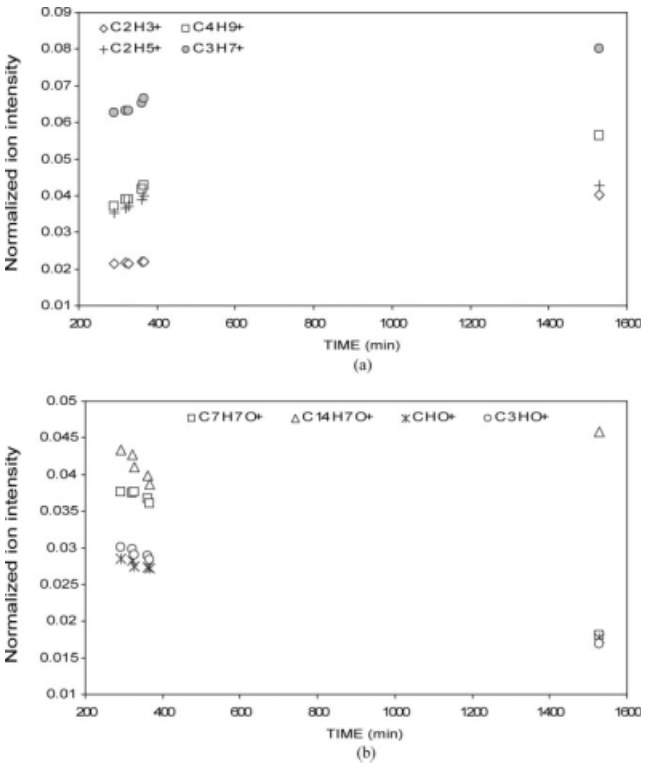

Figure 12 Variation in the intensity of secondary ion peaks of second and third domain samples that showed significant variance by PCA for (a) aliphatic hydrocarbon ions and (b) other ions.

with the most significant ion peak intensities that contributed to the variance captured by PC1 and PC2 being marked. Figure 12 shows the univariate plots of the ion peak intensities that had the most significant effect on the PCA loadings.

Figure 11(a) shows that the $C_7H_7O^+$ relative ion intensity contains the most significant variance. Aliphatic hydrocarbon groups $C_2H_3^+$, $C_4H_9^+$, $C_3H_7^+$, $C_4H_{11}^+$, $C_5H_9^+$, $C_4H_7^+$, and $C_6H_{13}^+$ made significant contributions to the loadings. A further contribution is noted from the CHO^+, CH_3O^+, and $C_3H_6N^+$ molecular ions. The aliphatic hydrocarbon ions are featured in the negative direction of the loading, and this explains their different trend in comparison with the $C_7H_7O^+$, CHO^+, and CH_3O^+ ions, which are featured on the opposite side of the loading plot, as a function of the curing reaction time. The significant aliphatic hydrocarbon ion variance indicates the establishment of the crosslinking reaction at this stage in time. Figure 12(a) shows that the most significant hydrocarbon ions increase rapidly as time increases. The $C_7H_7O^+$, CHO, and CH_3O^+ ions show a trend opposite of that of the hydrocarbon ions, as shown in Figure 12(b). Figure 11(b) shows that the $C_{14}H_7O^+$ ion is most significant in PC2 loadings. The univariate calibration of this ion [Fig. 12(c)] shows a trend similar to that of the samples in the PC2 score plot, and this suggests that this is the major event captured by PC2.

CONCLUSIONS

The progress of the curing reaction of an epoxy resin and diamine hardener has been followed successfully with ToF-SIMS. The ions that correspond to the curing reaction conversion have been identified. The blocking, coupling, and branching reaction steps occur at a faster rate than the crosslinking reaction. As the curing time progresses past the first domain of samples (>105 min), the reaction rate shifts in favor of the crosslinking reaction. The curing reaction conversion and the completion of the coupling and branching reaction steps can be established on the basis of the ion intensities of the aliphatic hydrocarbon, DGEBA/DGEBF hydroxyl, and aromatic ring-related ions. As the crosslinking reaction progresses, higher aliphatic and reduced hydroxyl ion intensities were observed. The cured resin crosslinking density can be indicated with the ratio of the relative ion intensities of the aliphatic hydrocarbon and hydroxyl ions.

References

1. Han, J. H.; Kim, C. G. Compos Struct 2006, 72, 218.
2. Williams, G.; Trask, R.; Bond, I. Compos A 2007, 38, 1525.
3. Penn, L. S.; Wang, H. In Handbook of Composites; Peters, S. T., Ed.; Chapman & Hall: London, 1998.
4. Ramírez, C.; Rico, M.; López, J.; Montero, B. J Appl Polym Sci 2007, 131, 1759.
5. Lahlali, D.; Naffakh, M.; Dumon, M. Polym Eng Sci 2005, 45, 1582.
6. Day, D. R.; Lewis, T. J.; Lee, H. L.; Senturia, S. D. J Adhes 1985, 18, 73.
7. Senturia, S. D.; Sheppard, N. F. Adv Polym Sci 1986, 80, 1.
8. Sung, C. S. P.; Mathisen, R. Polymer 1987, 28, 941.
9. Compton, D. A.; Hill, S. L.; Wright, N. A. Appl Spectrosc 1988, 42, 972.
10. Young, P. R.; Druy, M. A.; Stevenson, W. A.; Compton, D. A. C. SAMPE J 1989, 25, 11.
11. Myrick, M. L.; Angel, S. M.; Lyon, R. E, Vess, T. M. SAMPE J 1992, 28, 37.
12. Xu, D. M.; Zhang, K. D.; Zhu, X. L. J Appl Polym Sci 2006, 101, 3902.
13. Sharma, P.; Choudhary, V.; Narula, A. K. J Appl Polym Sci 2006, 101, 3503.
14. Pichaud, S.; Duteurtre, X.; Fit, A.; Stephan, F.; Maazouz, A.; Pascault, J. P. Polym Int 1999, 48, 1205.
15. Mercado, L. A.; Ribera, G.; Galia, M.; Cádiz, V. J Polym Sci Part A: Polym Chem 2006, 44, 1676.
16. Perrin, F. X.; Nguyen, T. M.; Vernet, J. L. Modeling Chem Phys 2007, 208, 55.
17. Omrani, A.; Ghaemy, M.; Rostami, A. A. Macromol Mater Eng 2006, 291, 181.
18. López-Quintela, A.; Prendes, P.; Pazos-Pellín, M.; Paz, M.; Paz-Abuín, S. Macromolecules 1998, 31, 4770.
19. Coullerez, G.; Leonard, D.; Lundmark, S.; Mathieu, H. J Surf Interface Anal 2000, 29, 431.

20. Rattana, A.; Abel, M. L.; Watts, J. F. Int J Adhes Adhes 2006, 26, 28.
21. Wagner, M. S.; Graham, D. J.; Ratner, B. D.; Castner, D. G. Surf Sci 2004, 570, 78.
22. Graham, D. J.; Wagner, M. S.; Castner, D. G. Appl Surf Sci 2006, 252, 6860.
23. Martens, H.; Naes, T. Multivariate Calibration; Wiley: London, 1989.
24. Awaja, F.; Daver, F.; Kosior, E. Polym Eng Sci 2004, 44, 1579.
25. Awaja, F.; Daver, F.; Kosior, E.; Cser, F. J Therm Anal Calorim 2004, 78, 865.
26. Inata, H.; Matsumura, S. J Appl Polym Sci 1985, 30, 3325.
27. Inata, H.; Matsumura, S. J Appl Polym Sci 1986, 32, 5193.
28. Inata, H.; Matsumura, S. J Appl Polym Sci 1986, 32, 4581.
29. Inata, H.; Matsumura, S. J Appl Polym Sci 1987, 33, 3069.
30. Inata, H.; Matsumura, S. J Appl Polym Sci 1987, 34, 2609.
31. Inata, H.; Matsumura, S. J Appl Polym Sci 1987, 34, 2769.
32. Leggett, G. J. In Wiley Static SIMS Library; Vickerman, J. C.; Briggs, D.; Henderson, A., Eds.; Surface Spectra: Manchester, United Kingdom, 1998; p 19.
33. Awaja, F.; van Riessen, G.; Pigram, P. J.; Fox, B.; Kelly, G. J Appl Polym Sci 2009, 113, 2755.